A facile approach to fabricating stretchable organic transistors with laser patterned Ag nanowire electrodes

*Runqiao Song,[1] Shanshan Yao,[1,2] Yuxuan Liu,[1] Hongyu Wang,[1] Jingyan Dong,[3] Yong Zhu,[1] Brendan T. O'Connor[1]**

1. Department of Mechanical and Aerospace Engineering, and Organic and Carbon Electronics Laboratories (ORaCEL), North Carolina State University, Raleigh, NC, 27695

2. Department of Mechanical Engineering, Stony Brook University, Stony Brook, NY, 11794

3. Department of Industrial and System Engineering, North Carolina State University, Raleigh, NC, 27695

* btoconno@ncsu.edu

Keywords: stretchable electronics, Ag nanowires, laser patterning, organic electronics, organic thin film transistors

Abstract

Stretchable electronics are poised to revolutionize personal healthcare and robotics where they enable distributed and conformal sensors. Transistors are fundamental building blocks of electronics and there is a need to produce stretchable transistors using low-cost and scalable fabrication techniques. Here, we introduce a facile fabrication approach using laser patterning and

transfer printing to achieve high-performance, solution-processed intrinsically stretchable organic thin-film transistors (OTFTs). The device consists of Ag NWs electrodes where the source and drain electrodes are patterned using laser ablation. The Ag NWs are then partially embedded in a polydimethylsiloxane (PDMS) matrix. The electrodes are combined with a PDMS dielectric and polymer semiconductor where the layers are individual transfer printed to complete the OTFT. Two polymer semiconductors, DPP-DTT and DPP-4T, are considered and show stable operation under cyclic strain of 20% and 40%, respectively. The OTFTs maintain electrical performance by adopting a buckled structure after the first stretch-release cycle. The conformability and stretchability of the OTFT is also demonstrated by operating the transistor while adhered to a finger being flexed. The ability to pattern highly conductive Ag NW networks using laser ablation to pattern electrodes as well as interconnects provides a simple strategy to produce complex stretchable OTFT-based circuits.

1. Introduction

Stretchable electronics can add valuable new functionality to a large variety of applications, including wearable health monitoring,[1–5] soft robotics,[6] and electronic skin.[7–9] Organic semiconductors[10–14] and nanomaterial-enabled conductors[15–19] are of particular interest due to their ability to be integrated into intrinsically stretchable platforms. While the organic semiconductors and nanomaterials are themselves not usually inherently elastomeric, through integration with elastomers that provide a restoring force upon stretching results in stretchable and electronically functional composites. Achieving intrinsic stretchability, where the entire device is able to stretch in an elastic fashion, allows for intimate and conformal contact to curvilinear, soft, and stretchable surfaces.[6,12] This attribute is beneficial in a number of ways, where for example, attaching to human skin would improve comfort and sensing performance. A primary device of interest is organic thin film transistors (OTFTs), which are fundamental building blocks of electronics and have been used to make stretchable sensors, displays and logic circuits.[10,12,20–22] To achieve intrinsically stretchable OTFTs, all components of the device need to be stretchable including the semiconductor, dielectric, and electrodes. To meet this need, there has been a considerable amount of research on achieving stretchable polymer semiconductors and semiconductor / elastomer composites. A variety of strategies have been employed from molecular design to improve deformability and elasticity,[23] to forming an interpenetrating network of polymer semiconductors in an elastomer matrix.[24–27] These approaches have led to a number of demonstrations of fully stretchable OTFTs.[6,12,23,24,26] In addition to the polymer semiconductor there is the need for stretchable electrodes and interconnects. Approaches to achieve intrinsically stretchable conductors that may be suitable as electrodes in OTFTs include the use of conductive polymers,[28–30] carbon nanotubes (CNTs),[16] and metallic nanowires (NWs),[19,31,32] as well as a number of other

nanomaterials.[33–35] CNTs and Ag NWs have been particularly successful when embedded in an elastomer matrix by forming a percolation network that can maintain electrical conductivity while being stretched.[36] While both approaches offer unique capabilities, Ag NWs exhibit higher conductivity and potentially lower cost.[16,37–39] As a result there has been interest in using Ag NWs to realize stretchable transistors. Liang et al. demonstrated a stretchable transistor with a semiconducting CNT channel and Ag NW electrodes spray coated through a shadow mask.[40] Lu et al. demonstrated a stretchable OTFT with spray coated Ag NWs.[41] In this demonstration the NWs were spray coated directly on the polymer semiconductor layer. However, when cyclically stretched by 40% strain the OTFT charge mobility was found to drop by over an order of magnitude in the strained state. Kim et al. demonstrated stretchable organic electrochemical transistors (OECTs) that employed Ag NWs with Au nanoparticles that were drop cast and patterned by lift-off using a kapton tape.[26] These reports demonstrate the potential of Ag NWs as an effective stretchable electrode. However, the processing methods have limitations. Spray coating requires compatibility of the solution with the surface its coating and the deposition quality is dependent on the ink viscosity, the evaporation rate, and the mask feature size. Using kapton tape in a lift off process demonstrated by Kim et al. would be challenging to scale up with high dimensional resolution. One could extrapolate the concept to photolithographic processing,[31] however this approach may result in unintended NW removal during photoresist lift-off, as well as concerns of cost.

Here, we report intrinsically stretchable OTFTs that can be stretched by over 40% strain and maintain consistent performance over a large number of stretching cycles. All components are intrinsically stretchable and solution processed. The electrodes consist of Ag NWs embedded in a polydimethylsiloxane (PDMS) matrix. Importantly, the source and drain electrodes are patterned

with a CO_2 laser providing a simple and scalable fabrication method. CO_2 lasers benefit from being low-cost and provides precise pattern control.[42,43] The laser ablation of the NWs was performed on quartz substrates, which significantly improves pattern quality relative to soda lime glass and plastics. Two conjugated polymers are considered for the semiconductor layer, DPP-DTT and DPP-4T, with molecular structure shown in **Figure 1**. These polymers were chosen given their ductility and high charge mobility.[12,27,44] Finally, the OTFT dielectric was a thin layer of PDMS. Each of the device layers are processed on a separate substrate and then transfer printing is used to produce stand-alone stretchable OTFTs. The use of transfer printing provides a simple route to fabricate the devices where each layer can be separately optimized and then brought together during device fabrication. For example, transfer printing allows for the electrodes to be processed separately where the NWs initially buried under a PDMS matrix can be reoriented as necessary to make efficient electrical contact with other device layers. The use of transfer printing also overcomes the difficulty of casting the polymer semiconductor solution on the hydrophobic elastomer. We show that the stretchable OTFTs have a charge mobility similar to OTFTs fabricated on silicon substrates. Furthermore, the DPP-4T based stretchable OTFTs can maintain consistent charge mobility that is comparable to the unstrained device while undergoing cyclic strain of 40%. We probe the structure of the OTFT with confocal laser scanning microscopy (CLSM) and scanning electron microscopy (SEM). During the initial strain and release process, the OTFT forms a buckled structure, driven largely by the Ag NW / PDMS composite. Upon additional strain cycles the buckling morphology remains stable. While the OTFT buckles the layers are found to remain well adhered under the applied cyclic strain, resulting in consistent OTFT performance. Finally, we laminate the stretchable OTFT onto a finger and use it to switch on and off an LED while the finger bends, demonstrating the potential in wearable electronics.

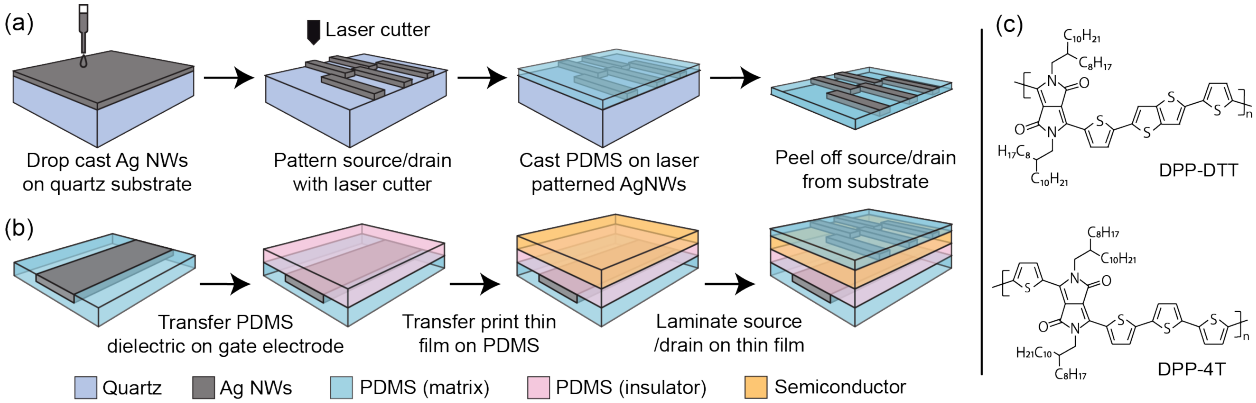

Figure 1. (a) Schematic of the fabrication of the source / drain composite electrode. (b) Schematic of the OTFT device assembly. (c) The molecular structure of the polymer semiconductors DPP-DTT and DPP-4T used in the OTFTs.

2. Results and Discussion

2.1. Electrode fabrication

The stretchable OTFTs have a bottom gate top contact architecture, with the fabrication procedure illustrated in **Figure 1**. The fabrication begins with producing the Ag NW / PDMS composite electrodes. For the source and drain electrodes, the Ag NWs were drop cast on a quartz substrate. An SEM image of the drop cast Ag NW conductive network is shown in **Figure 2(a)**. The Ag NW network was then patterned using CO_2 laser ablation. A CO_2 laser was chosen due to its wide-availability and low-cost. The power of the CO_2 laser can also be finely tuned to precisely ablate the NWs with good pattern resolution. Fused quartz was chosen over soda lime glass as the substrate due to its low thermal expansion coefficient allowing for laser ablation of the NWs without fracturing the substrate due to thermal shock. Both glass and fused quartz absorb light at the 10.6 μm laser wavelength, which results in heating the substrate. However, the thermal expansion coefficient of fused quartz (0.54×10^{-6}/K) is more than an order of magnitude lower than

glass ($9.35x10^{-6}$/K).[45–47] When using glass as the substrate, crack formation was clearly visible as shown in **Figure 2(c,d)** and **Figure S1(a-c)**. In comparison, the quartz substrate remains stable during the cutting process without crack formation as shown in **Figure 2(e,f)** and **Figure S1(d-f)**. Also, as shown in **Figure 2(b,d)**, the edge quality is significantly improved when going from glass to quartz. Alternative substrates were also considered that included silicon, polyimide (PI), and polyethylene terephthalate (PET). Silicon has a lower absorption coefficient at the 10.6 μm laser wavelength, however, due to high laser reflection it was not employed for safety reasons. Plastic substrates including PI and PET were burned easily by the CO_2 laser making them unsuitable.

The pattern control of CO_2 laser ablation was explored by varying the processing parameters of the laser including the laser power and raster speed, with results given in **Figure S2**. The maximum laser power and speed are 60 W and 25.4 cm/s, respectively. It was found that as the laser power increased the width of the removed Ag NW network increased, and as the raster speed increased the width of the ablated NWs decreased. For the lowest power (20%) and highest speed (60%) considered, the width of the cut was found to be approximately 120 μm wide. While this is sufficient for device demonstration, reducing the channel length and improving the pattern resolution would improve transistor speed and reduce device dimensions that may be required for a given application. To go beyond the nominal 75 μm spot size limit of the laser, we used a combination of a metallic shadow mask with the laser cutter to ablate the NWs with a width of approximately 30 μm, as shown in **Figure S3**. While further work is required to improve the pattern quality, it is possible to achieve relatively narrow line widths with a CO_2 laser cutter. To improve the pattern resolution further, alternative laser cutters such as a UV laser or Ti:Saphire laser have been shown to ablate Ag NW networks with a resolution of 5 μm or less.[48,49]

For device fabrication, we used a laser power (30%) and speed (60%) that resulted in a 150 μm channel length as pictured in **Figure 3(b)**. The width of source/drain electrodes was then made to be 1 mm wide, as shown in **Figure 2(f)**. After the Ag NWs were patterned PDMS was drop cast on the NWs and the Ag NW / PDMS composite was cured. The PDMS thickness was approximate 50 μm. Similarly, the gate electrode was produced by drop casting a layer of Ag NWs on a glass substrate followed by drop casting the PDMS. Once the composites were peeled off the donor substrate the Ag NWs were partially exposed at the surface of the film, allowing for high electrical conductivity, good electrical contact with the remainder of the device, and were mechanically robust.

2.2. Assembling the OTFT

Following the fabrication of the electrodes, the dielectric layer and polymer semiconductor layer were spin coated on separate substrates. The PDMS was spin coated on polystyrene sulfonate (PSS) coated glass, while DPP-DTT and DPP-4T films was spin coated on octyltrichlorosilane (OTS) treated glass. By processing each layer on a separate substrate the film quality was significantly improved. The thicknesses of the PDMS film and the semiconductor thin films were approximately 3.5 μm and 25 nm, respectively. The OTFT was then assembled as illustrated in **Figure 1(b)**, which started by attaching the Ag NW / PDMS composite that acts as the gate electrode to a custom strain stage, which would later be used to test device stretchability. The PDMS dielectric layer that was coated on the PSS coated glass substrate was then laminated to the gate electrode composite. Prior to laminating the PDMS dielectric, the gate electrode was UV ozone (UVO) treated for 5 minutes to promote the adhesion between the gate electrode and the dielectric layer.[44] The stack was then immersed in deionized (DI) water, where the PSS dissolved and the glass substrate was removed leaving the PDMS dielectric on the gate electrode. The polymer semiconductor film on

the OTS-treated glass was then laminated to the PDMS dielectric. The glass substrate was quickly removed leaving the polymer semiconductor attached to the dielectric layer.[50,51] During the transfer printing process, the polymer semiconductor layer may be damaged, impacting device performance. We performed atomic force microscopy (AFM) images of the DPP-4T films as cast on the donor substrate and after transfer printing on the PDMS dielectric, with results given in **Figure S4**. While we scan opposite sides of the film with this process, we find that the film quality is roughly equivalent, consistent with our previous demonstrations of transfer printed polymer semiconductors.[52,53] Finally, the source-drain electrodes that consist of the Ag NW / PDMS composite were removed from its donor quartz substrate and laminated onto the polymer semiconductor layer.

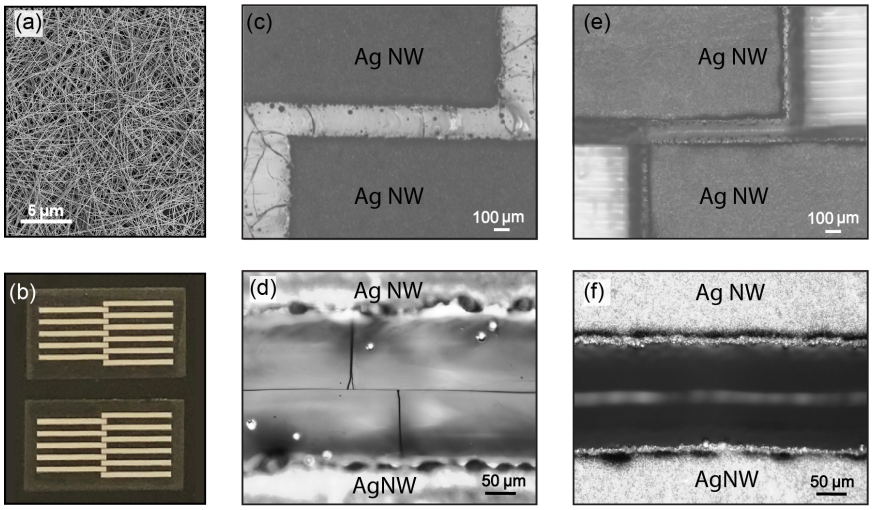

Figure 2. (a) SEM image of drop cast Ag NW networks on a quartz substrate. (b) A picture of Ag NW / PDMS source/drain electrodes patterned by laser cutting after peeling off from the quartz substrate. (c,d) Optical microscope images of the OTFT source-drain channel fabricated by laser patterning the Ag NW network on a glass substrate. (e,f) Optical microscope image of the OTFT source-drain channel fabricated by laser patterning on a quartz substrate.

2.3. Electrical Characterization

Prior to characterizing the OTFTs, we studied the electrical conductivity of the Ag NW / PDMS composite while being stretched. The sheet resistance of the composite was measured as a function of strain, as shown in **Figure 3**. As the composite was strained to 100%, the sheet resistance increased from 1.3 to 4.5 Ohm/sq. When the strain was released, the sheet resistance dropped slightly but remained similar to that measured at the maximum applied strain, as shown in **Figure 3(a)**. The normalized sheet resistance of the composite when cyclically strained by 20% and 40% is given in **Figure 3(b)**. These strains were chosen as they were the same used for the stretchable OTFTs, to be discussed. For both the 20% and 40% strain cases, the sheet resistance repeatedly increased in the strained state and decreased in the released state, but remained less than 3 Ohm/sq. The sheet resistance in both the strained and released states remained relatively constant over 100 strain cycles. These results are consistent with previous Ag NW / PDMS composite results where the resistance increased with the strain, but then remained stable under cyclic strain.[32]

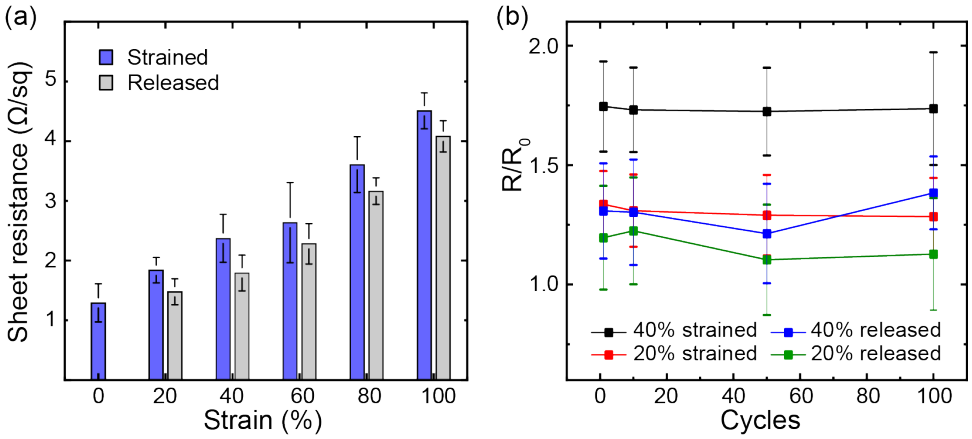

Figure 3. (a) Sheet resistance of the Ag NW / PDMS composite when strained and strained then released to its unstrained state. (b) The change in sheet resistance relative to the unstrained sheet resistance (R_0) under cyclic strain when strained by 20% and 40% with sheet resistance given in the strained state and released state.

The limiting strain range of the OTFTs is dictated by the structural stability of the device. We limited the applied strain on the devices to below the fracture strain (or crack onset strain (COS)) of the polymer semiconductor layers. While there have been demonstrations of stretchable OTFTs functioning beyond their COS,[11] we do not consider that case here. The COS of DPP-DTT and DPP-4T were found to be approximately 25% and 80%, respectively. In addition to this constraint is the need for all device layers to remain well adhered under cyclic straining. We found that for the DPP-4T based stretchable OTFT, the layers would delaminate under a cyclic strain of 60%. Thus, to limit polymer semiconductor fracture, the DPP-DTT based OTFTs were strained to 20% strain, and to limit delamination, the DPP4T based OTFTs were strained to 40% strain.

Before being stretched, the DPP-DTT based stretchable OTFTs had an average saturated field effect mobility of 0.285 ± 0.031 $cm^2V^{-1}s^{-1}$ with the maximum mobility of 0.345 $cm^2V^{-1}s^{-1}$, with the current voltage characteristics and mobility given in **Figure 4(a-c)**. The measured charge mobility was found to be only marginally below that measured on a silicon OTFT test bed, which was measured to be 0.499 ± 0.098 $cm^2V^{-1}s^{-1}$ with the current voltage characteristics shown in **Figure S5(a)**. Under applied uniaxial strain the transistor characteristics were measured with the channel length parallel and perpendicular to the applied strain direction, with results given in **Figure 4(a,b)** and **Figure S6**, and the extracted charge mobility given in **Figure 4(c)**. It was found that the charge mobility dropped slightly during the first few strain cycles and then remained relatively stable. For the charge transport perpendicular to the strain direction, the drop in mobility was less than 30% of that in the unstrained device. The charge mobility was also found to be similar in the strained and released states. The decrease in the charge mobility was greater for the charge transport parallel to the strain direction. In this case, the charge mobility had a slow decay with strain cycles in the strained state, while in the released state there was an immediate drop in

charge mobility that was then stable with further stretching cycles. The observed drop in mobility is likely associated with the buckled structure adopted by the OTFT during the stretching/releasing process. Overall, the charge mobility remained quite stable for charge transport both parallel and perpendicular to the strain direction. After 100 stretching cycles the charge mobility remained at approximately 0.10 $cm^2V^{-1}s^{-1}$ when charge transport was parallel to the strain direction and remained above 0.2 $cm^2V^{-1}s^{-1}$ when charge transport was perpendicular to the strain direction.

Next, the more ductile DPP-4T based stretchable OTFTs were measured when strained by 40%. The stretchable OTFT in the unstrained state had an average of charge mobility 0.113± 0.033 $cm^2V^{-1}s^{-1}$ with a maximum of 0.154 $cm^2V^{-1}s^{-1}$. The current-voltage characteristics are given in **Figure 4(d-f)** and **Figure S7**. The mobility compared quite well to OTFTs fabricated on silicon substrates, which had a charge mobility of 0.150 ± 0.041 $cm^2V^{-1}s^{-1}$, with the current-voltage characteristics shown in **Figure S5(b)**. Similar to the DPP-DTT devices, the DPP-4T OTFTs had a drop in charge mobility after the first stretching cycle, as shown in **Figure 4(f)**. After the first stretching cycle, the current-voltage characteristics remained similar with further stretching cycles as shown in **Figure S7**. The consistent electrical characteristics resulted in similar charge mobility indicative of good device stability. Unlike the DPP-DTT OTFTs, the charge mobility parallel to the channel length in the strained state showed remarkable stability with little drop in charge mobility with cyclic stretching. It is known that the DPP-4T is more ductile than DPP-DTT owing to the greater conformation freedom associated with the thiophene moieties linked by C-C bonds along the backbone. The ductile DPP-4T may accommodate larger applied strain without significantly reducing the molecular packing order, resulting in an ability to maintain nearly constant charge mobility.[53,54] In addition, the drop in charge mobility for transport perpendicular to the strain direction may be associated with greater polymer backbone alignment in the direction

of strain, given the higher applied strains relative to the DPPDTT OTFTs.[53] This will results in increased π-π intermolecular charge transport that is widely accepted to be poorer than intramolecular charge transport along the polymer backbone.[53] When the strain is released the mobility was found to drop for charge transport parallel and perpendicular to the strain direction. This is attributed to greater wrinkling in the device, potentially resulting in a non-uniform electric field applied across the channel.

In these stretchable OTFTs, it is worth noting that the current-voltage characteristics were well behaved showing minimal hysteresis and without major non-idealities.[55] In addition, while there is some signature of contact resistance with both polymer semiconductors, as observed through the small non-linear current-voltage curves at low applied voltage in the output characteristics (i.e s-shape) shown in **Figure 4(b,e)**, the contact resistance does not dominate the behavior and the curves show good saturation at higher source-drain voltages. This is partly attributed to the use of a thick Ag NW network used for the source and drain electrodes. The ability to use relatively thick Ag NW layers that are then embedded in PDMS provides a simple route to ensure a flat surface with good electric conductivity to contact to the polymer semiconductor layer. Finally, the ability of the device to function under large strains was demonstrated by using the OTFT as a switch to operate an LED when the OTFT was attached to a flexing finger, as shown in **Figure 5**. As the finger was flexed a tensile strain was applied to the OTFT. A video capturing the device operation is provided in the supporting information showing stable LED performance as the finger was flexed, highlighting the potential use in wearable electronic applications.

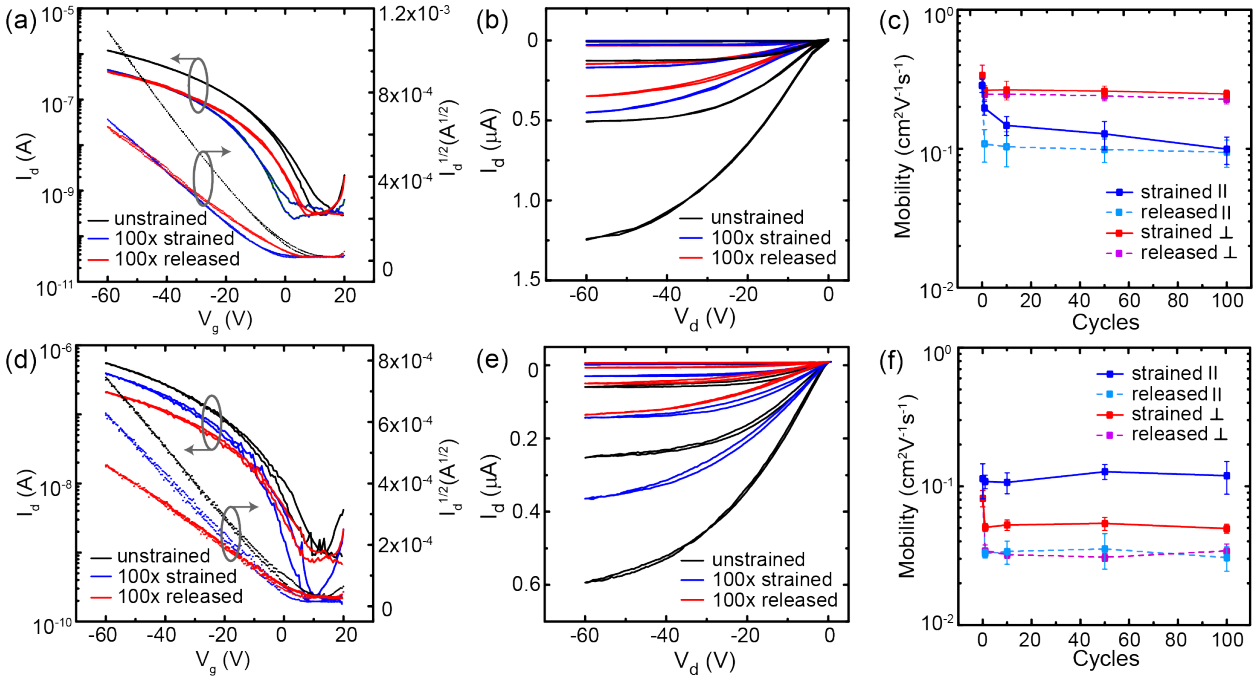

Figure 4. (a) The transfer curves and (b) output curves for a characteristic DPP-DTT based stretchable OTFT for charge transport parallel to the applied strain direction. The measurements include an unstrained film and after 100 strain cycles at 20% applied strain when measured in the strained state and the strain released state. The output curves are given with a gate voltage of 0 V, -20 V, and -40 V. (c) Charge mobility of the DPP-DTT OTFT with cyclic strain in the 20% strained state and strain released state for charge transport parallel (∥) and perpendicular (⊥) to the direction on strain. (d) The transfer curves and (e) the output curves for characteristics DPP-4T OTFT for charge transport parallel to the strain direction. (f) Charge mobility of the DPP-4T OTFT with cyclic strain in the 40% strained state and strain released state.

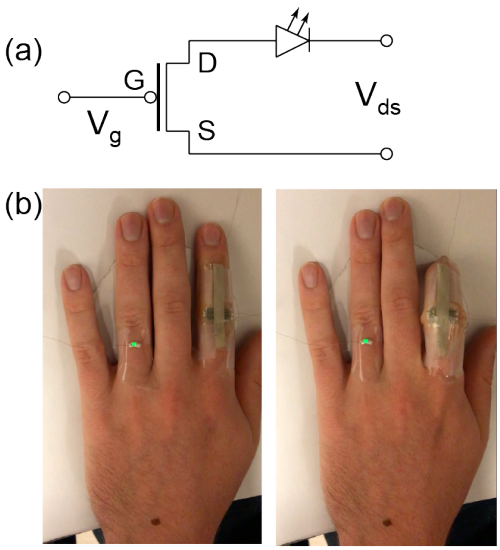

Figure 5. (a) Schematic of OTFT and LED circuit. (b) Picture of a green LED being switched on by the stretchable OTFT while adhered to a flexing finger. A video showing stable operation of the LED during finger flexure is given in the supporting information.

2.4. Structural Stability

To understand the OTFT performance during the cyclic straining process, the structural integrity of the device was probed. To start, we considered the behavior of a PDMS / Ag NW / PDMS composite. In this case a thin PDMS dielectric film was laminated on the Ag NW / PDMS composite mimicking a partially fabricated OTFT. This setup allowed us to observe the wrinkling behavior of the NWs from above the film, which was not possible for a fully fabricated OTFT. The surface of the unstrained sample was smooth with a roughness of 0.7 μm (**Figure S8**). When the composite was strained and released, buckles formed on the surface of the composite. The buckling of the composite was measured by CLSM under varying stretching cycles with the images given in **Figure 6**, and **Figure S9**.

The buckling is due to the irreversible sliding of the Ag NWs in the PDMS composite during the stretching cycle. When the composite is stretched, the Ag NWs slide to accommodate the strain. Upon strain removal the PDMS elastomer provides a restoring force while the stiffer Ag NWs

resist compression and result in a buckling instability.[32,56] This buckling process and irreversible movement of the NWs results in an initial increase in electrical resistance of the composite as shown in **Figure 3**. After the first several straining cycles the composite finds a stable buckled microstructure (**Figure S9**) that then leads to a stable electrical resistance. We find that there are buckles both perpendicular and parallel to the strain direction. As the composite is strained the buckles parallel to the strain direction are found to increase in height, as pointed by arrows in **Figure 6(a)**. This behavior is attributed to the transverse compression on the sample when under uniaxial tensile strain due to the Poisson's ratio. As shown in **Figure S9**, the buckling behavior is highly reversible with additional strain cycles. The buckling behavior with the straining cycles is consistent with the electrical characteristics that show stable device behavior in the strained and released states with increasing stretching cycles.

Cross-sectional SEM images of the PDMS / Ag NW / PDMS composite that was similar in structure to that imaged by CLSM is given in **Figure 6(c)**. Here, the composite was imaged after being cyclically strained to 40% for 100 cycles. In addition, a cross-sectional view of a fully fabricated DPP-4T stretchable OTFT that was cyclically stretched to 40% for 100 cycles is given in **Figure 6(d)**. In the images, there are small gaps that can be observed between the layers. These gaps are attributed to the cutting process used to expose the edge of the device for imaging and are not believed to be delamination. As can be seen, particularly in **Figure 6(c)**, the layers converged just beneath the exposed surface, suggesting that the layers remain adhered during the cyclic strain process. In these images, the wrinkling behavior of the NWs composite is clearly visible and is consistent with the CLSM images of the surface of the partially fabricated OTFT.

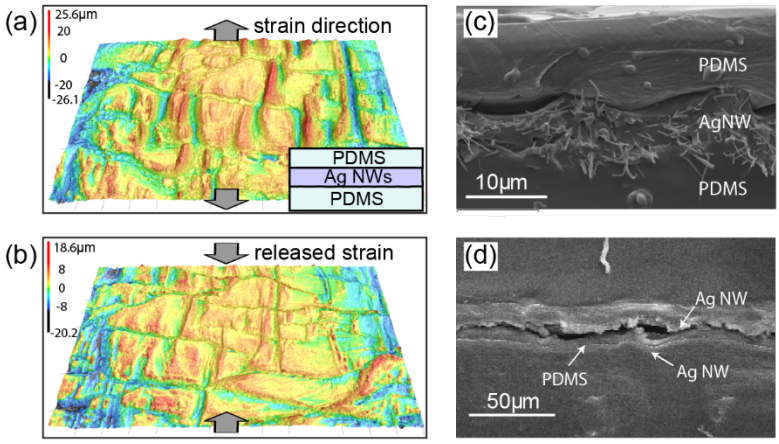

Figure 6. Confocal laser scanning microscope images of PDMS/ Ag NW/ PDMS (~50 µm / ~4 µm / ~4 µm) strained by 20% (a), and then released (b) after 100 strain cycles. The inset of (a) includes an illustration of the composite stack. The strain direction was in the vertical direction of the page. (c) SEM image of the cross-section of a PDMS / Ag NW / PDMS composite that has been cyclically stretched for 100 cycles by 40% strain. (d) SEM image of the cross section of a DPP-4T based stretchable OTFT in the strain-released state after 100 cycles of 40% strain.

3. Conclusion

A simple approach to fabricate high performance intrinsically stretchable OTFTs was demonstrated. Key to the device fabrication is that each layer was individually processed on separate substrates that was then transfer printed to assemble the OTFT. Ag NWs were chosen as the electrodes due to their high conductivity and stretchability when embedded in a PDMS matrix. The source and drain electrodes were patterned using CO_2 laser ablation, providing a simple cost-effective and scalable strategy to pattern the devices. The pattern quality was found to be significantly improved when using quartz substrates over glass owing to its lower thermal expansion coefficient. This patterning approach may be expanded to not only pattern the OTFT channel but also pattern Ag NW interconnects, providing a simple strategy for fabricating stretchable circuits. The fabricated OTFTs were shown to remain stable when strained cyclically

by up to 40% strain. The devices have stable well-behaved current voltage characteristics with little hysteresis and low contact resistance demonstrating the potential for Ag NW electrodes in stretchable OTFTs. This is the first demonstration that integrates Ag NWs and polymer semiconductors that show this level of stability at the applied strains considered. Embedding the Ag NWs in the PDMS elastomer for the gate and source-drain electrodes provides a natural encapsulation on both sides of the device assisting in making the devices thin and stable. In addition, stretchable OTFTs with stable performance were achieved using a simple neat polymer semiconductor film. The device stability is attributed to a stable buckling morphology that forms during the cyclic strain process, driven primarily by the buckling of the Ag NW / PDMS composite. This buckling behavior was clearly observed using CLSM and SEM imaging. Finally, the stretchable transistors were able to function as an LED switching unit when attached to a flexing finger illustrating its potential for wearable electronics. These results demonstrate the use of laser patterning and transfer printing that provide a simple fabrication approach to achieve high performance stretchable transistors.

4. Experimental Methods

Materials and synthesis

Polydimethylsiloxane (PDMS, SYLGARD 184) was purchased from Ellsworth. DPP-DTT with molecular weight of 292,200 kg/mol and DPP-4T with molecular weight of 171,138 kDa were purchased from Ossila. Quartz substrates were purchased from swift glass, and the glass was purchased from Fisher Scientific. The Ag NWs were synthesized through a modified polyol process.[57] First, 60 mL of a 0.147 M poly(vinylpyrrolidone) (PVP) solution in ethylene glycol (EG) was added to a round-bottom flask to which a stir bar was added. The flask was suspended in an oil bath and heated to a temperature of 155 °C for 1 h under magnetic stirring at a speed of 250

rpm. After 15 min, 200 μL of a 24 M $CuCl_2$ solution in EG was injected into the PVP solution. The solution was then heated for an additional 15 min, followed by injecting 60 mL of a 0.094 M $AgNO_3$ solution in EG. The mixed solution was heated for another 1.5 hours. After cooling down, the Ag NWs were purified by centrifuging in ethanol and acetone repeatedly. The average diameter and length of the resulted Ag NWs are around 60 nm and 20 μm, respectively.

Fabrication of stretchable transistors

The stretchable transistor was fabricated by separately solution casting each of the active layers and then assembling through transfer printing, as illustrated in **Figure 2(b)**. To prepare the gate, source, and drain electrodes, Ag NWs were dispersed in ethanol with a concentration of 8 mg/ml. The solution was drop-cast on a quartz substrate pre-heated at 50 °C, followed by thermally annealing the Ag NW film at 100 °C for 20 min on a hot plate in ambient. The source and drain electrodes were then patterned by a CO_2 laser cutter (VersaLASER, VLS6.60) with 1,000 pulses/in. The channel length was set to 150 μm and channel width was 1000 μm. PDMS with a base to cross-linker ratio of 15:1 by weight was then drop cast on the source and drain electrodes. For the gate electrodes the drop cast Ag NWs were patterned into a 6 mm width strip and then the PDMS was drop cast on the NWs. In both cases the PDMS was cured in a vacuum oven (2.67 kPa) at 80 °C for 6 hours. The gate dielectric was made by mixing 30 wt% PDMS with hexane, stirring for 30 min and removing the air bubbles in an evacuated chamber for 20 min. The PDMS mixture had a base to cross-linker ratio of 15:1 by weight. The PDMS solution was spun cast on a PSS coated glass substrate with a 2-step spin coating procedure that included 2,000 rpm for 15 s followed by 5,000 rpm for 60 s. The PDMS film was then cured at 170 °C for 50 min. The DPP-DTT and DPP-4T semiconductor films were prepared by first dissolving the polymer in chloroform at a concentration of 4 mg/ml. The solutions were spun cast on OTS-treated glass

substrate at 1500 rpm for 60 seconds, followed by annealing at 150 °C for 10 min in a nitrogen filled glove box. The assembly of the layers to fabricate the stretchable transistors is described above. The fabrication of the control non-stretchable OTFT was prepared by spin coating the DPP-DTT and DPP-4T solution directly on transistor test beds that were then annealed at 150 ^{o}C for 10 minutes. The transistor test bed consisted of a p-type Silicon wafer with a 300 nm thermal oxide layer that acted as the gate dielectric. The source and drain electrodes were composed of thermally evaporated Ti/ Au (10 nm/ 40 nm) patterned by photolithography to form a channel length that varied from 50 μm to 100 μm and a channel width of 1000 μm. The test beds were OTS treated prior to coating the polymer semiconductor layer. OTS treatment was prepared by first cleaning the substrates in DI-water, acetone and isopropanol for 15 minutes each. The substrates were UVO treated for 15 minutes and plasma treated for 2 minutes. The substrates were then put in a solution with 110 ml of hexadecane and 50 μl of OTS for 16 hours. After 16 hours, the substrates were removed from the solution and cleaned in chloroform, isopropanol, and DI-water. Finally, the substrates were annealed at 150 ^{o}C for 10 minutes.

Device and material characterization

To identify the COS, 30 nm thick polymer films were transfer printed onto a 1 mm thick PDMS slab clamped on a custom strain stage. The polymer / PDMS stack was strained while being observed under an optical microscope. The COS was considered to be the first observed fractures in the film. A semiconductor polymer analyzer (HP4156b) was used for both sheet resistance and transistor characterization. The field effect mobility was extracted from taking the slope in the transfer curves over a 10 V range. In this case, the source-drain voltage was held at 60 V. In determining the charge mobility when the devices were stretched, the change in channel length were taken into account by measuring the change in channel length with strain. The dielectric

constant of the PDMS thin film used for the mobility calculation was 2.84 that was measured by an impedance analyzer from 40 Hz to 50 kHz at room temperature, as shown in **Figure S10**. The dielectric constant was extracted from the capacitance measurement by using $C = \kappa\varepsilon_0 \frac{d}{A}$. The thickness of the polymer semiconductor films and PDMS (dielectrics) were measured by ellipsometry (J.A. Woollam). All electrical measurements were conducted in the ambient environment. The uncertainty was based on the standard deviation of at least 8 samples.

The images of the composite buckling were taken by a Keyence VKx1100 CLSM. The SEM images of the composite cross-section were taken with a variable pressure Hitachi 3200 SEM. To prepare the sample for SEM, the devices were first laminated on a styrene plate, epoxy was then spread on the devices and cured by UV light for 10 min. The sample was then soaked in liquid nitrogen and cut by a liquid nitrogen cooled razor blade. The sample was attached to a SEM holder and coated with Au and then placed into the SEM. The images of DPP-4T films before and after transfer printing were taken by Park XE-70 AFM using non-contact mode.

ASSOCIATED CONTENT

Supporting Information: Optical microscope images of the laser patterned Ag NW electrodes, OTFT electrical characteristics, CLSM images of the stretchable composites, and capacitance measurement for the PDMS dielectric. A video of stretchable OTFT switching an LED.

ACKNOWLEDGMENT

The authors gratefully acknowledge support for this research through NSF award 1728370. The authors thank Dr. Xiaojing Jiang for assistance with their impedance analyzer.

REFERENCES

(1) Yamamoto, Y.; Harada, S.; Yamamoto, D.; Honda, W.; Arie, T.; Akita, S.; Takei, K. Printed Multifunctional Flexible Device with an Integrated Motion Sensor for Health Care Monitoring. *Sci. Adv.* **2016**, *2* (11), e1601473–e1601473. https://doi.org/10.1126/sciadv.1601473.

(2) Son, D.; Kang, J.; Vardoulis, O.; Kim, Y.; Matsuhisa, N.; Oh, J. Y.; To, J. W.; Mun, J.; Katsumata, T.; Liu, Y.; McGuire, A.; Krason, M.; Molina-Lopez, F.; Ham, J.; Kraft, U.; Lee, Y.; Yun, Y.; Tok, J.B.-H.; Bao, Z. An Integrated Self-Healable Electronic Skin System Fabricated via Dynamic Reconstruction of a Nanostructured Conducting Network. *Nat. Nanotechnol.* **2018**, *13* (11), 1057–1065. https://doi.org/10.1038/s41565-018-0244-6.

(3) Koo, J. H.; Jeong, S.; Shim, H. J.; Son, D.; Kim, J.; Kim, D. C.; Choi, S.; Hong, J. I.; Kim, D. H. Wearable Electrocardiogram Monitor Using Carbon Nanotube Electronics and Color-Tunable Organic Light-Emitting Diodes. *ACS Nano* **2017**, *11* (10), 10032–10041. https://doi.org/10.1021/acsnano.7b04292.

(4) Trung, T. Q.; Ramasundaram, S.; Hwang, B.; Lee, N. An All-Elastomeric Transparent and Stretchable Temperature Sensor for Body-Attachable Wearable Electronics. *Adv. Mater.* **2016**, *28*, 502–509. https://doi.org/10.1002/adma.201504441.

(5) Yao, S.; Swetha, P.; Zhu, Y. Nanomaterial-Enabled Wearable Sensors for Healthcare. *Adv. Healthc. Mater.* **2018**, *7* (1), 1–27. https://doi.org/10.1002/adhm.201700889.

(6) Kim, H.-J.; Yu, C.; Sim, K.; Rao, Z.; Thukral, A.; Shim, H. Fully Rubbery Integrated Electronics from High Effective Mobility Intrinsically Stretchable Semiconductors. *Sci. Adv.* **2019**, *5* (2), eaav5749. https://doi.org/10.1126/sciadv.aav5749.

(7) Wang, C.; Hwang, D.; Yu, Z.; Takei, K.; Park, J.; Chen, T.; Ma, B.; Javey, A. User-

Interactive Electronic Skin for Instantaneous Pressure Visualization. *Nat. Mater.* **2013**, *12* (10), 899–904. https://doi.org/10.1038/nmat3711.

(8) Boutry, C. M.; Negre, M.; Jorda, M.; Vardoulis, O.; Chortos, A.; Khatib, O.; Bao, Z. A Hierarchically Patterned, Bioinspired e-Skin Able to Detect the Direction of Applied Pressure for Robotics. *Sci. Robot.* **2018**, *6914* (November), 1–10.

(9) Molina-Lopez, F.; Gao, T. Z.; Kraft, U.; Zhu, C.; Öhlund, T.; Pfattner, R.; Feig, V. R.; Kim, Y.; Wang, S.; Yun, Y.; Bao, Z. Inkjet-Printed Stretchable and Low Voltage Synaptic Transistor Array. *Nat. Commun.* **2019**, *10* (1), 1–10. https://doi.org/10.1038/s41467-019-10569-3.

(10) Oh, J. Y.; Rondeau-Gagné, S.; Chiu, Y. C.; Chortos, A.; Lissel, F.; Wang, G. J. N.; Schroeder, B. C.; Kurosawa, T.; Lopez, J.; Katsumata, T.; Xu, J.; Zhu, C.; Gu, X.; Bae, W.-G.; Kim, Y.; Jin, L.; Chung, J.W.; Ok, J.B.-H.; Bao, Z. Intrinsically Stretchable and Healable Semiconducting Polymer for Organic Transistors. *Nature* **2016**, *539* (7629), 411–415. https://doi.org/10.1038/nature20102.

(11) Chortos, A.; Lim, J.; To, J. W. F.; Vosgueritchian, M.; Dusseault, T. J.; Kim, T. H.; Hwang, S.; Bao, Z. Highly Stretchable Transistors Using a Microcracked Organic Semiconductor. *Adv. Mater.* **2014**, *26* (25), 4253–4259. https://doi.org/10.1002/adma.201305462.

(12) Wang, S.; Xu, J.; Wang, W.; Wang, G. J. N.; Rastak, R.; Molina-Lopez, F.; Chung, J. W.; Niu, S.; Feig, V. R.; Lopez, J.; Lei, T.; Kwon, S.-K.; Kim, Y.; Foudeh, A.M.; Ehrlich, A.; Gasperini, A.; Yun, Y.; Murmann, B.; Tok, J.B.-H.; Bao, Z. Skin Electronics from Scalable Fabrication of an Intrinsically Stretchable Transistor Array. *Nature* **2018**, *555* (7694), 83–88. https://doi.org/10.1038/nature25494.

(13) Zhu, C.; Wu, H.-C.; Nyikayaramba, G.; Bao, Z.; Murmann, B. Intrinsically Stretchable Temperature Sensor Based on Organic Thin-Film Transistors. *IEEE Electron Device Lett.* **2019**, *40* (10), 1630–1633. https://doi.org/10.1109/led.2019.2933838.

(14) Song, R.; Schrickx, H.; Balar, N.; Siddika, S.; Sheikh, N.; O'Connor, B. T. Unveiling the Stress-Strain Behavior of Conjugated Polymer Thin Films for Stretchable Device Applications. *Macromolecules* **2020**, *53* (6), 1988–1997. https://doi.org/10.1021/acs.macromol.9b02573.

(15) Kim, K. S.; Zhao, Y.; Jang, H.; Lee, S. Y.; Kim, J. M.; Kim, K. S.; Ahn, J. H.; Kim, P.; Choi, J. Y.; Hong, B. H. Large-Scale Pattern Growth of Graphene Films for Stretchable Transparent Electrodes. *Nature* **2009**, *457* (7230), 706–710. https://doi.org/10.1038/nature07719.

(16) Lipomi, D. J.; Vosgueritchian, M.; Tee, B. C. K.; Hellstrom, S. L.; Lee, J. A.; Fox, C. H.; Bao, Z. Skin-like Pressure and Strain Sensors Based on Transparent Elastic Films of Carbon Nanotubes. *Nat. Nanotechnol.* **2011**, *6* (12), 788–792. https://doi.org/10.1038/nnano.2011.184.

(17) Chortos, A.; Koleilat, G. I.; Pfattner, R.; Kong, D.; Lin, P.; Nur, R.; Lei, T.; Wang, H.; Liu, N.; Lai, Y. C.; Kim, M.-G.; Chung, J.W.; Lee, S.; Bao, Z. Mechanically Durable and Highly Stretchable Transistors Employing Carbon Nanotube Semiconductor and Electrodes. *Adv. Mater.* **2016**, *28* (22), 4441–4448. https://doi.org/10.1002/adma.201501828.

(18) Kim, D. H.; Yu, K. C.; Kim, Y.; Kim, J. W. Highly Stretchable and Mechanically Stable Transparent Electrode Based on Composite of Silver Nanowires and Polyurethane-Urea. *ACS Appl. Mater. Interfaces* **2015**, *7* (28), 15214–15222.

https://doi.org/10.1021/acsami.5b04693.

(19) Yao, S.; Zhu, Y. Wearable Multifunctional Sensors Using Printed Stretchable Conductors Made of Silver Nanowires. *Nanoscale* **2014**, *6* (4), 2345–2352. https://doi.org/10.1039/c3nr05496a.

(20) Jung, S. W.; Choi, Z. J. S.; Koo, J. B.; Park, C. W.; Na, B. S.; Oh, J. Y.; Lee, S. S.; Chu, H. Y. Stretchable Organic Thin-Film Transistors Fabricated on Elastomer Substrates Using Polyimide Stiff-Island Structures. *ECS Solid State Lett.* **2014**, *4* (1), P1–P3. https://doi.org/10.1149/2.0011501ssl.

(21) Reeder, J.; Kaltenbrunner, M.; Ware, T.; Arreaga-Salas, D.; Avendano-Bolivar, A.; Yokota, T.; Inoue, Y.; Sekino, M.; Voit, W.; Sekitani, T.; Someya, T. Mechanically Adaptive Organic Transistors for Implantable Electronics. *Adv. Mater.* **2014**, *26* (29), 4967–4973. https://doi.org/10.1002/adma.201400420.

(22) Yokota, T.; Sekitani, T.; Tokuhara, T.; Take, N.; Zschieschang, U.; Klauk, H.; Takimiya, K.; Huang, T. C.; Takamiya, M.; Sakurai, T.; Someya, T. Sheet-Type Flexible Organic Active Matrix Amplifier System Using Pseudo-CMOS Circuits with Floating-Gate Structure. *IEEE Trans. Electron Devices* **2012**, *59* (12), 3434–3441. https://doi.org/10.1109/TED.2012.2220853.

(23) Mun, J.; Kang, J.; Zheng, Y.; Luo, S.; Wu, H.; Matsuhisa, N.; Xu, J.; Wang, G. N.; Yun, Y.; Xue, G.; Tok, J.B.-H.; Bao, Z. Conjugated Carbon Cyclic Nanorings as Additives for Intrinsically Stretchable Semiconducting Polymers. *Adv. Mater.* **2019**, *1903912*, 1903912. https://doi.org/10.1002/adma.201903912.

(24) Song, E.; Kang, B.; Choi, H. H.; Sin, D. H.; Lee, H.; Lee, W. H.; Cho, K. Stretchable and Transparent Organic Semiconducting Thin Film with Conjugated Polymer Nanowires

Embedded in an Elastomeric Matrix. *Adv. Electron. Mater.* **2016**, *2* (1), 1–8. https://doi.org/10.1002/aelm.201500250.

(25) Choi, D.; Kim, H.; Persson, N.; Chu, P. H.; Chang, M.; Kang, J. H.; Graham, S.; Reichmanis, E. Elastomer-Polymer Semiconductor Blends for High-Performance Stretchable Charge Transport Networks. *Chem. Mater.* **2016**, *28* (4), 1196–1204. https://doi.org/10.1021/acs.chemmater.5b04804.

(26) Kim, H. J.; Sim, K.; Thukral, A.; Yu, C. Rubbery Electronics and Sensors from Intrinsically Stretchable Elastomeric Composites of Semiconductors and Conductors. *Sci. Adv.* **2017**, *3* (9), 1–9. https://doi.org/10.1126/sciadv.1701114.

(27) Xu, J.; Wang, S.; Wang, G. N.; Zhu, C.; Luo, S.; Jin, L.; Gu, X.; Chen, S.; Feig, V. R.; To, J. W. F.; Rondeua-Gagne, S.; Park, J.; Schroeder, B.C.; Lu, C.; Oh, J.Y.; Wnag, Y.; Kim, Y.-H.; Yan, H.; Sinclair, R.; Zhou, D.; Xue, G.; Murmann, B.; Linder, C.; Cai, W.; Tok, J.B.-H.; Chung, J.W.; Bao, Z. Highly Stretchable Polymer Semiconductor Films through the Nanoconfinement Effect. *Science (80-.).* **2017**, *64*, 59–64.

(28) Lipomi, D. J.; Lee, J. A.; Vosgueritchian, M.; Tee, B. C.-K.; Bolander, J. A.; Bao, Z. Electronic Properties of Transparent Conductive Films of PEDOT:PSS on Stretchable Substrates. *Chem. Mater.* **2011**, *24*, 373–382.

(29) Kayser, L. V.; Lipomi, D. J. Stretchable Conductive Polymers and Composites Based on PEDOT and PEDOT:PSS. *Adv. Mater.* **2019**, *1806133*, 1806133. https://doi.org/10.1002/adma.201806133.

(30) White, M. S.; Kaltenbrunner, M.; Głowacki, E. D.; Gutnichenko, K.; Kettlgruber, G.; Graz, I.; Aazou, S.; Ulbricht, C.; Egbe, D. A. M.; Miron, M. C.; Major, M.; Scharber, M.C.; Sekitani, T.; Someya, T.; Bauer, S.; Sariciftci, N.S. Ultrathin, Highly Flexible and

Stretchable PLEDs. *Nat. Photonics* **2013**, *7* (10), 811–816. https://doi.org/10.1038/nphoton.2013.188.

(31) Zhu, B.; Gong, S.; Lin, F.; Wang, Y.; Ling, Y.; An, T.; Cheng, W. Patterning Vertically Grown Gold Nanowire Electrodes for Intrinsically Stretchable Organic Transistors. *Adv. Electron. Mater.* **2019**, *5* (1), 1–6. https://doi.org/10.1002/aelm.201800509.

(32) Xu, F.; Zhu, Y. Highly Conductive and Stretchable Silver Nanowire Conductors. **2012**, 5117–5122. https://doi.org/10.1002/adma.201201886.

(33) Sun, Q.; Kim, D. H.; Park, S. S.; Lee, N. Y.; Zhang, Y.; Lee, J. H.; Cho, K.; Cho, J. H. Transparent, Low-Power Pressure Sensor Matrix Based on Coplanar-Gate Graphene Transistors. *Adv. Mater.* **2014**, *26* (27), 4735–4740. https://doi.org/10.1002/adma.201400918.

(34) Yao, S.; Ren, P.; Song, R.; Liu, Y.; Huang, Q.; Dong, J.; O'Connor, B. T.; Zhu, Y. Nanomaterial-Enabled Flexible and Stretchable Sensing Systems: Processing, Integration, and Applications. *Adv. Mater.* **2019**, *1902343*, 1902343. https://doi.org/10.1002/adma.201902343.

(35) Ho, D. H.; Sun, Q.; Kim, S. Y.; Han, J. T.; Kim, D. H.; Cho, J. H. Stretchable and Multimodal All Graphene Electronic Skin. *Advanced Materials*. 2016, pp 2601–2608. https://doi.org/10.1002/adma.201505739.

(36) Yao, S.; Zhu, Y. Nanomaterial-Enabled Stretchable Conductors: Strategies, Materials and Devices. *Adv. Mater.* **2015**, *27* (9), 1480–1511. https://doi.org/10.1002/adma.201404446.

(37) Lee, Y.; Oh, J. Y.; Xu, W.; Kim, O.; Kim, T. R.; Kang, J.; Kim, Y.; Son, D.; Tok, J. B.; Park, M. J. Stretchable Organic Optoelectronic Sensorimotor Synapse. *Sci. Adv.* **2018**, No. November, 1–10.

(38) Yu, Z.; Niu, X.; Liu, Z.; Pei, Q. Intrinsically Stretchable Polymer Light-Emitting Devices Using Carbon Nanotube-Polymer Composite Electrodes. *Adv. Mater.* **2011**, *23* (34), 3989–3994. https://doi.org/10.1002/adma.201101986.

(39) Park, S.; Vosguerichian, M.; Bao, Z. A Review of Fabrication and Applications of Carbon Nanotube Film-Based Flexible Electronics. *Nanoscale* **2013**, *5* (5), 1727–1752. https://doi.org/10.1039/c3nr33560g.

(40) Liang, J.; Li, L.; Chen, D.; Hajagos, T.; Ren, Z.; Chou, S. Y.; Hu, W.; Pei, Q. Intrinsically Stretchable and Transparent Thin-Film Transistors Based on Printable Silver Nanowires, Carbon Nanotubes and an Elastomeric Dielectric. *Nat. Commun.* **2015**, *6* (May). https://doi.org/10.1038/ncomms8647.

(41) Lu, C.; Lee, W. Y.; Shih, C. C.; Wen, M. Y.; Chen, W. C. Stretchable Polymer Dielectrics for Low-Voltage-Driven Field-Effect Transistors. *ACS Appl. Mater. Interfaces* **2017**, *9* (30), 25522–25532. https://doi.org/10.1021/acsami.7b06765.

(42) Marchiori, B.; Delattre, R.; Hannah, S.; Blayac, S.; Ramuz, M. Laser-Patterned Metallic Interconnections for All Stretchable Organic Electrochemical Transistors. *Sci. Rep.* **2018**, *8* (1), 1–9. https://doi.org/10.1038/s41598-018-26731-8.

(43) Guo, F.; Kubis, P.; Przybilla, T.; Spiecker, E.; Hollmann, A.; Langner, S.; Forberich, K.; Brabec, C. J. Nanowire Interconnects for Printed Large-Area Semitransparent Organic Photovoltaic Modules. *Adv. Energy Mater.* **2015**, *5* (12). https://doi.org/10.1002/aenm.201401779.

(44) Sun, T.; Song, R.; Balar, N.; Sen, P.; Kline, R. J.; O'Connor, B. T. Impact of Substrate Characteristics on Stretchable Polymer Semiconductor Behavior. *ACS Appl. Mater. Interfaces* **2019**, *11* (3), 3280–3289. https://doi.org/10.1021/acsami.8b16457.

(45) Ohdaira, K.; Fujiwara, T.; Endo, Y.; Nishizaki, S.; Matsumura, H. Formation of Several-Micrometer-Thick Polycrystalline Silicon Films on Soda Lime Glass by Flash Lamp Annealing. *Jpn. J. Appl. Phys.* **2008**, *47* (11), 8239–8242. https://doi.org/10.1143/JJAP.47.8239.

(46) Merritt, G. E. Thermal Expansion of Fused Quartz. *J. Am. Ceram. Soc.* **1924**, *7* (11), 803–808. https://doi.org/10.1111/j.1151-2916.1924.tb18174.x.(47) Kikuchi, Y.; Sudo, H.; Kuzuu, N. Thermal Expansion of Vitreous Silica: Correspondence between Dilatation Curve and Phase Transitions in Crystalline Silica. *J. Appl. Phys.* **1997**, *82* (8), 4121–4123. https://doi.org/10.1063/1.366279.

(48) Liang, C.; Sun, X.; Zheng, J.; Su, W.; Hu, Y.; Duan, J. Surface Ablation Thresholds of Femtosecond Laser Micropatterning Silver Nanowires Network on Flexible Substrate. *Microelectron. Eng*. **2020**, *232* ,111396. https://doi.org/10.1016/j.mee.2020.111396.

(49) Pan, C. T.; Yang, T. L.; Wang, S. Y.; Yen, C. K.; Ju, S. P.; Huang, C.W.; Shiue, Y. L.; Study on Optical Films with AgNWs Using UV Laser Patterning. *Opt. Master*. **2018**, *77* ,55-66. https://doi.org/10.1016/j.optmat.2018.01.016

(50) O'Connor, B.T.; Kline, R. J.; Conrad, B. R.; Richter, L. J.; Gundlach, D.; Toney, M. F.; DeLongchamp, D. M. Anisotropic Structure and Charge Transport in Highly Strain-Aligned Regioregular Poly(3-Hexylthiophene). *Adv. Funct. Mater.* **2011**, *21* (19), 3697–3705. https://doi.org/10.1002/adfm.201100904.

(51) Meitl, M. A.; Zhu, Z. T.; Kumar, V.; Lee, K. J.; Feng, X.; Huang, Y. Y.; Adesida, I.; Nuzzo, R. G.; Rogers, J. A. Transfer Printing by Kinetic Control of Adhesion to an Elastomeric Stamp. *Nat. Mater.* **2006**, *5* (1), 33–38. https://doi.org/10.1038/nmat1532.

(52) Sen, P.; Xiong, Y.; Zhang, Q.; Park, S.; You, W.; Ade, H.; Kudenov, M. W.; O'Connor,

B. T. Shear-Enhanced Transfer Printing of Conducting Polymer Thin Films. ACS Appl. Mater. Interfaces 2018, *10* (37), 31560–31567. https://doi.org/10.1021/acsami.8b09968.

(53) Sun, T.; Scott, J. I.; Wang, M.; Kline, R. J.; Bazan, G. C.; O'Connor, B. T. Plastic Deformation of Polymer Blends as a Means to Achieve Stretchable Organic Transistors. *Adv. Electron. Mater.* **2017**, *3* (1), 1–10. https://doi.org/10.1002/aelm.201600388.

(54) Balar, N.; Siddika, S.; Kashani, S.; Peng, Z.; Rech, J. J.; Ye, L.; You, W.; Ade, H.; O'Connor, B. T. The Role of Secondary Thermal Relaxations in Conjugated Polymer Film Toughness. *Chem. Mater.* **2020**, acs.chemmater.0c01910. https://doi.org/10.1021/acs.chemmater.0c01910.

(55) Choi, H. H.; Cho, K.; Frisbie, C. D.; Sirringhaus, H.; Podzorov, V. Critical Assessment of Charge Mobility Extraction in FETs. *Nat. Mater.* **2017**, *17* (1), 2–7. https://doi.org/10.1038/nmat5035.

(56) Zhu, Y.; Qin, Q.; Xu, F.; Fan, F.; Ding, Y.; Zhang, T.; Wiley, B. J.; Wang, Z. L. Size Effects on Elasticity, Yielding, and Fracture of Silver Nanowires: In Situ Experiments. *Phys. Rev. B - Condens. Matter Mater. Phys.* **2012**, *85* (4), 1–7. https://doi.org/10.1103/PhysRevB.85.045443.

(57) Korte, K. E.; Skrabalak, S. E.; Xia, Y. Rapid Synthesis of Silver Nanowires through a CuCl- or CuCl2-Mediated Polyol Process. *J. Mater. Chem.* **2008**, *18* (4), 437–441. https://doi.org/10.1039/b714072j.

Table of Content Figure